

RESEARCH ARTICLE | JUNE 22 2021

## Liquid structure and dynamics in the choline acetate:urea 1:2 deep eutectic solvent

Special Collection: Chemical Physics of Deep Eutectic Solvents

Alessandro Triolo  ; Maria Enrica Di Pietro; Andrea Mele; Fabrizio Lo Celso ; Martin Brehm ;  
Valerio Di Lisio; Andrea Martinelli ; Philip Chater ; Olga Russina 

 Check for updates

*J. Chem. Phys.* 154, 244501 (2021)

<https://doi.org/10.1063/5.0054048>



View  
Online

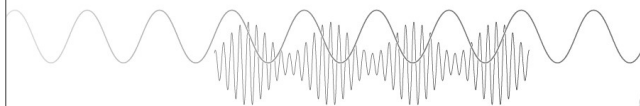


Export  
Citation

CrossMark

Webinar

Boost Your Signal-to-Noise  
Ratio with Lock-in Detection



Sep. 7th – Register now



Zurich  
Instruments

# Liquid structure and dynamics in the choline acetate:urea 1:2 deep eutectic solvent

Cite as: J. Chem. Phys. 154, 244501 (2021); doi: 10.1063/5.0054048

Submitted: 14 April 2021 • Accepted: 7 June 2021 •

Published Online: 22 June 2021



View Online



Export Citation



CrossMark

Alessandro Triolo,<sup>1,a)</sup> Maria Enrica Di Pietro,<sup>2</sup> Andrea Mele,<sup>2</sup> Fabrizio Lo Celso,<sup>1,3</sup> Martin Brehm,<sup>4</sup> Valerio Di Lisio,<sup>5</sup> Andrea Martinelli,<sup>5</sup> Philip Chater,<sup>6</sup> and Olga Russina<sup>1,5,a)</sup>

## AFFILIATIONS

<sup>1</sup>Laboratorio Liquidi Ionici, Istituto Struttura della Materia, Consiglio Nazionale delle Ricerche (ISM-CNR), Rome, Italy

<sup>2</sup>Department of Chemistry, Materials and Chemical Engineering "G. Natta," Politecnico di Milano, Milano, Italy

<sup>3</sup>Department of Physics and Chemistry, Università di Palermo, Palermo, Italy

<sup>4</sup>Institut für Chemie, Martin-Luther-Universität Halle-Wittenberg, Halle (Saale), Germany

<sup>5</sup>Department of Chemistry, University of Rome Sapienza, Rome, Italy

<sup>6</sup>Diamond House, Harwell Science and Innovation Campus, Diamond Light Source, Ltd., Didcot, Oxfordshire OX11 0DE, United Kingdom

**Note:** This paper is part of the JCP Special Topic on Chemical Physics of Deep Eutectic Solvents.

<sup>a)</sup> **Authors to whom correspondence should be addressed:** triolo@ism.cnr.it and olga.russina@uniroma1.it

## ABSTRACT

We report on the thermodynamic, structural, and dynamic properties of a recently proposed deep eutectic solvent, formed by choline acetate (ChAc) and urea (U) at the stoichiometric ratio 1:2, hereinafter indicated as ChAc:U. Although the crystalline phase melts at 36–38 °C depending on the heating rate, ChAc:U can be easily supercooled at sub-ambient conditions, thus maintaining at the liquid state, with a glass–liquid transition at about –50 °C. Synchrotron high energy x-ray scattering experiments provide the experimental data for supporting a reverse Monte Carlo analysis to extract structural information at the atomistic level. This exploration of the liquid structure of ChAc:U reveals the major role played by hydrogen bonding in determining interspecies correlations: both acetate and urea are strong hydrogen bond acceptor sites, while both choline hydroxyl and urea act as HB donors. All ChAc:U moieties are involved in mutual interactions, with acetate and urea strongly interacting through hydrogen bonding, while choline being mostly involved in van der Waals mediated interactions. Such a structural situation is mirrored by the dynamic evidences obtained by means of <sup>1</sup>H nuclear magnetic resonance techniques, which show how urea and acetate species experience higher translational activation energy than choline, fingerprinting their stronger commitments into the extended hydrogen bonding network established in ChAc:U.

© 2021 Author(s). All article content, except where otherwise noted, is licensed under a Creative Commons Attribution (CC BY) license (<http://creativecommons.org/licenses/by/4.0/>). <https://doi.org/10.1063/5.0054048>

## INTRODUCTION

In the last decade, large interest has been grown around deep eutectic solvents (DESs)<sup>1,2</sup> and their applications in several fields.<sup>3–8</sup> After the classification of DES in terms of four different types proposed by Smith *et al.*,<sup>3</sup> those belonging to type III are among the most commonly encountered ones. These latter DESs are composed of a mixture of a salt {e.g., choline [i.e., (2-hydroxyethyl)-trimethylammonium cation] chloride} with a hydrogen bonding donor (such as urea and glycerol) with, depending on the concentration ratio between the two components, a melting point depression resulting from their mixing. The large interest on these compounds

stems from several appealing properties, not least their cheap production cost and easy preparation and purification. Most of them are also characterized by nonflammability, bio-compatibility, and low toxicity, thus turning out to be ideal media for the development of a variety of processes. On the other hand, most of these appealing features stem from the combination of chemical–physical properties of different components. Accordingly, by making (even minor) changes to their chemical nature, one can efficiently modulate the resulting macroscopic performance, thus leading to the classification of DES as task-specific solvents.<sup>4</sup> Among the most well-known DESs, we recall the stoichiometric 1:2 mixture of choline chloride (CC) and urea (U), sometimes referred to as reline.<sup>9–16</sup>

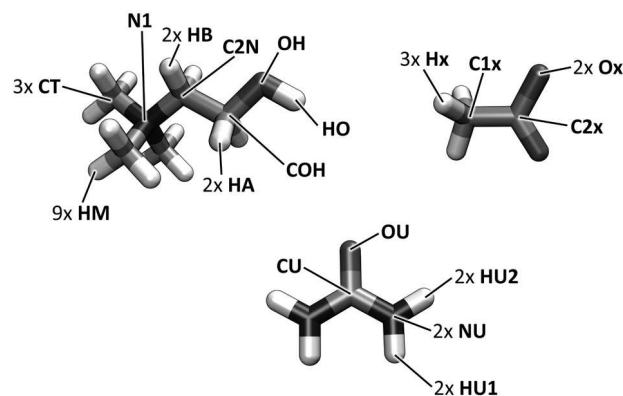
Dry reline melts at  $\sim 31^\circ\text{C}$ <sup>17</sup> and has attracted huge interest over the last few years. Other CC-based DESs have been proposed, including CC-glycerol (Gly) 1:2 (glyceline),<sup>18–22</sup> CC-ethylene glycol (EG) 1:2 (ethaline),<sup>22–24</sup> and, more recently, CC-water 1:3.3–4.2 (aquoline).<sup>25–27</sup> The recent interest in DESs stems from the opportunity that they provide to modulate their solvating properties by changing their chemical composition. Aiming at expanding the spectrum of properties, other anions paired with choline have been explored as well. For example, choline acetate (ChAc) has recently been considered as an interesting ionic liquid to be paired with an HB donor to lead to a DES. ChAc is an ionic liquid with melting point at  $51^\circ\text{C}$ , proposed by Fukaya *et al.*, as an interesting example of an IL solely composed of biomaterials.<sup>28</sup> The opportunity to use it as a salt for preparation of a DES was presented by Zhao *et al.*, who showed the eutectic nature of mixtures of ChAc with urea (1:2), Gly, and EG; these DESs showed low viscosity, high biodegradability, and excellent compatibility with lipase.<sup>29</sup> More recently, ChAc mixtures with different HBDs were probed for their efficiency toward enzymatic reaction with  $\beta$ -galactosidase.<sup>30</sup> In 2020, some of us used ChAc-based DES in order to efficiently solubilize hemicellulose at mild conditions.<sup>31</sup>

This intense applicative activity calls for a deeper understanding of the chemical–physical properties of ChAc-based DESs that have so far received negligible attention compared, e.g., to their CC-based equivalents. Here, we present a detailed experimental and computational study of structural and dynamic properties of the DES composed of ChAc and urea at 1:2M ratio, hereinafter indicated as ChAc:U. The structural properties of ChAc:U have been obtained by merging high energy x-ray diffraction and a reverse Monte Carlo computational approach, aiming at extracting the atomistic level structural details of the liquid organization in bulk. The sample has also been probed with nuclear magnetic resonance (NMR) techniques, aiming at extracting dynamic information related to rotational and translational processes, occurring around room temperature. Overall, this study provides a careful characterization of structural and dynamic properties of a new, eco-sustainable DES, paving the way for its application as a complementary medium to other related DESs.

## EXPERIMENTAL AND COMPUTATIONAL DETAILS

Choline acetate (ChAc) used for differential scanning calorimetry (DSC) and x-ray scattering was a TCI product; urea was a Sigma-Aldrich product. ChAc and urea were dried under vacuum at ambient temperature for several days. Eutectic mixtures at 1:2 ChAc:U ratio were prepared in a glovebox with an inert atmosphere to reduce ambient moisture contamination, leading to ChAc:U formation (see Scheme 1). After mixing, the sealed vials were kept at  $40^\circ\text{C}$  under constant agitation for at least one hour to lead to a transparent homogeneous liquid. The sample could be maintained amorphous when kept at ambient temperature ( $20^\circ\text{C}$ ) in thin sealed capillaries; it would crystallize when kept inside large sealed vials.

DSC thermograms were acquired by using a Mettler Toledo DSC 822e equipped with a FRS5 sensor and a liquid nitrogen cooler. The furnace was purged during the measurement with dry nitrogen at a flow rate of  $30\text{ ml min}^{-1}$ . A sample of about 5 mg was weighted in a  $40\ \mu\text{l}$  aluminum pan and rapidly sealed. DSC scans involve



**SCHEME 1.** Schematic representation of choline (top, left), acetate (top, right), and urea (bottom) moieties of ChAc:U (choline acetate:urea = 1:2). The nomenclature of the different atomic species is shown.

cooling from  $50$  to  $-125^\circ\text{C}$  followed by heating from  $-125$  up to  $50^\circ\text{C}$ , with a heating/cooling rate of  $2/10^\circ\text{C min}^{-1}$ .

Warm, liquid ChAc:U was loaded into a borosilicate capillary of 1.5 mm outer diameter, which was glue-sealed. After this operation, the sample maintained liquid even at ambient temperature ( $\sim 20^\circ\text{C}$ ). The total high-resolution x-ray scattering data were collected on the I15-1 beamline at Diamond Light Source, UK, using x rays of wavelength  $0.309\ 574\ \text{\AA}$  and a Perkin Elmer XRD 4343 CT detector. The total scattering data were integrated to 1D using DAWN<sup>32</sup> and then normalized and corrected to extract  $S(Q)$  using GudrunX.<sup>33,34</sup>

ChAc and U for NMR experiments were purchased from Iolitec and Sigma-Aldrich, respectively, and used without further purification. The DES at 1:2M ratio was prepared by using the heating method, by mixing the two constituents at  $80^\circ\text{C}$  under stirring for 1 h, until a homogeneous and transparent liquid was formed. As neither freshly prepared ChAc:U nor its starting components were dried, a residual amount of water is present in the sample (5.7 wt. % by Karl Fischer titration). Controlled amounts of water are beneficial to reduce the viscosity and allow for satisfactorily resolved NMR spectra. The sample was transferred to a 5 mm NMR tube, equipped with a capillary containing DMSO- $d_6$ . NMR measurements were performed at 11.74 T NMR with a Bruker NEO 500 console equipped with a direct observe BBFO (broadband including fluorine) iProbe (a  $^1\text{H}$  resonance frequency of 500.13 MHz). Measurements were performed over a temperature range of 278–358 K in 5 K increments, and a minimum of 15 min allowed for thermal equilibration. The residual amount of water together with the tendency of liquid to remain in a supercooled state when slowly cooled (see the section titled RESULTS and DISCUSSION) allowed for NMR measurements at such temperatures.

$T_1$  relaxation measurements were carried out without sample spinning with the inversion recovery (IR) pulse sequence using relaxation delays at least five times the longest  $T_1$ , and the instrument was carefully tuned and shimmed, and the  $90^\circ$  pulses were calibrated before each measurement. The spin-lattice relaxation rates were measured using data matrices of  $16\ 384\ (t_2) \times 16\ (t_1)$ , over a spectral width of 9 ppm for various delay times  $\tau$ , ranging from 0.05–5 to 0.05–12 s, according to the temperature. A total of two transients per increment were collected for each  $T_1$  experiment. The

baselines of all arrayed  $T_1$  spectra were corrected prior to processing the data, and integrals were used to calculate relaxation times. A single exponential decay was observed for all samples over the entire temperature range investigated. Relaxation times were computed from experimental raw data by means of the Bruker  $T_1/T_2$  relaxation module using the manual integration option and applying the standard one-component fitting function. Data were processed three times, and errors were calculated from the maximum standard deviation found at the lowest temperature. Maximum errors are estimated to be 1%. Fits to extract the correlation times and rotational activation energies from the relaxation rates were performed with OriginPro 2018 using a user-defined function with the Levenberg–Marquardt algorithm. For the fit procedure, average errors were estimated to be 5%.

Self-diffusion coefficients were measured by pulsed field gradient (PFG) experiments by applying sine-shaped pulsed magnetic field gradients along the  $z$  direction up to a maximum strength of  $G = 53.5 \text{ G cm}^{-1}$ . All the diffusion experiments were performed using the bipolar pulse longitudinal eddy current delay (BPP-LED) pulse sequence. All experiments were carried out over a spectral width of 9 ppm, with a total of eight transients per increment. The relaxation delay was set to at least five times  $T_1$ , and four dummy scans were programmed prior to acquisition. The pulse gradients were incremented from 2% to 95% of the maximum gradient strength in a linear ramp with 32 steps. For each DOSY experiment, the duration of the magnetic field pulse gradients ( $\delta$ ) and the diffusion times ( $\Delta$ ) were optimized to obtain, where possible, 95% signal attenuation for the slowest diffusion species at the last step experiment.  $\delta$  values were in the 2.4–6 ms range, while  $\Delta$  values were 0.4–0.8 s long. The baselines of all arrayed spectra were corrected prior to processing the data. Data were processed using an exponential filter in F2 dimension ( $LB = 0.3 \text{ Hz}$ ), and integrals were used in calculating relaxation times. The determination of self-diffusion coefficients used the Bruker  $T_1/T_2$  module of Topspin for each peak. The precision of the measured diffusion coefficients is estimated to be within 3%.

2D  $^1\text{H}$ – $^1\text{H}$  nuclear Overhauser enhancement (NOESY) experiments were recorded at 298 K by using the phase-sensitive ge-2D NOESY pulse sequence using echo-antiecho (noesyetgp in the Bruker library). Spectra were recorded using eight transients over  $4096 (t_2) \times 256 (t_1)$  complex data points. 32 dummy scans and mixing times in the range 20–500 ms were used. The relaxation delay was set to 4 s. The NOESY datasets were processed by applying a sine-squared window function in both dimensions ( $SSB = 2$ ) prior to the Fourier transform.

The EPSR approach has been used to model the x-ray diffraction data.<sup>35</sup> This is a robust reverse Monte Carlo approach (using a NVT ensemble) that is based on the optimization of the empirically proposed potential that leads to the best agreement with experimental diffraction data.

We used a simulation box containing 100 ChAc ion pairs and 200 urea moieties (ChAc:Urea = 1:2) with a density of  $1.17 \text{ g/cc}^{30}$  (cubic box size =  $35.3 \text{ \AA}$ ) at  $25 \text{ }^\circ\text{C}$ . The starting interatomic potential used for choline and urea is the one that was successfully used by Hammond *et al.* in their study of reline.<sup>10,36</sup> The acetate interaction potential parameters are the same used by Bowron *et al.* in their study of acetate based ionic liquids.<sup>37</sup> The used parameters are reported in the supplementary material. After an equilibration

of  $\sim 6000$  steps, the EPSR was activated and further 10 000 steps delivered a good agreement of the calculated diffraction pattern with the experimental one. At this stage, further 7000 steps were collected to achieve statistical accuracy on the structural observables (pair distribution functions and angular distributions). In order to evaluate structural properties from the resulting Monte Carlo trajectories, the TRAVIS software was used.<sup>38–40</sup>

## RESULTS AND DISCUSSION

The DSC trace of ChAc:U is shown in Fig. 1, where two thermal traces are shown with heating/cooling rates equal to 2 and  $10 \text{ }^\circ\text{C min}^{-1}$ , respectively. It appears that ChAc:U, if cooled from the melt state, can be easily supercooled, maintaining in the liquid state and eventually converting into a glass, without crystallization intervening. The liquid–glass transition ( $T_g$ ) can be detected in a small temperature range between  $-48$  and  $-50 \text{ }^\circ\text{C}$  in both cooling and heating stages. On the other hand, upon heating the glass, cold-crystallization ( $T_{cc}$ ) occurs at 6 and  $19 \text{ }^\circ\text{C}$  depending on the heating rate. Soon after, the crystalline phase of ChAc:U melts at  $T_m = 36 \text{ }^\circ\text{C}$  at  $2 \text{ }^\circ\text{C min}^{-1}$  or at  $T_m = 38 \text{ }^\circ\text{C}$  at  $10 \text{ }^\circ\text{C min}^{-1}$ .

It is noteworthy that, upon cooling from the melt, ChAc:U remains in the liquid supercooled state at  $20 \text{ }^\circ\text{C}$  for long time (several days). Accordingly, we determined the liquid structure of ChAc:U at ambient temperature, without incurring into sample crystallization during the experiment time duration. Synchrotron x-ray diffraction data collected in such a way are reported in Fig. 2. It appears that ChAc:U is characterized by an x-ray diffraction pattern similar to the ones from other choline-based DESs, such as reline and aquoline.<sup>10,11,21,24,27,41–43</sup>

The quality of the agreement of the experimental x-ray scattering pattern and the corresponding EPSR-computed quantity is shown in Fig. 2. The EPSR-derived x-ray weighted scattering pattern nicely accounts for the experimentally observed features, thus providing a validation support to the structural information that can be extracted from the computed trajectories. It can be appreciated

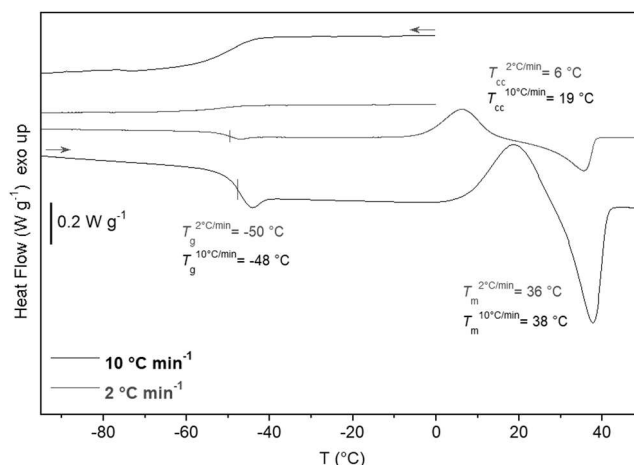


**FIG. 1.** Thermal traces of ChAc:U recorded at two different heating/cooling rates (2 and  $10 \text{ }^\circ\text{C min}^{-1}$ , respectively). Indications of the liquid–glass transition ( $T_g$ ), cold-crystallization ( $T_{cc}$ ), and crystal melting ( $T_m$ ) are highlighted.

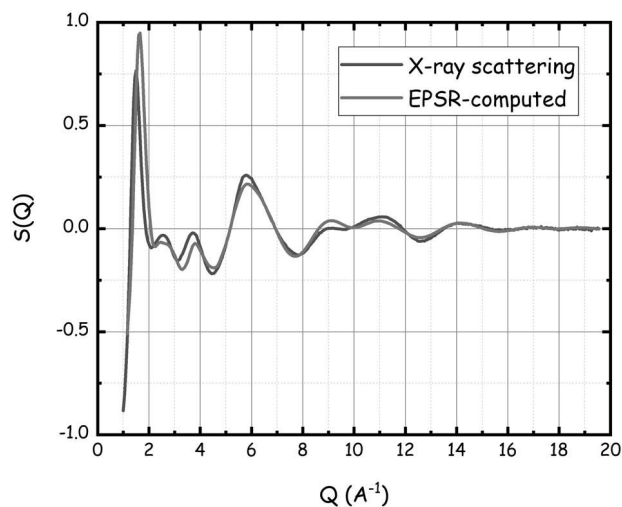


**FIG. 2.** Comparison between experimental (black) and EPSR-computed (red) x-ray scattering patterns from ChAc:U at ambient temperature.

that similarly to other choline-based DESs,<sup>10,11,21,24,27,41–43</sup> the experimental x-ray scattering pattern does not show appreciable features at low  $Q$  values, apart from the low  $Q$  peak at  $\sim 1.5 \text{ \AA}^{-1}$ , thus suggesting that no large scale structural heterogeneities occur in this system, which could be related either to polar/apolar segregation<sup>44–47</sup> or to mesoscopic phase separation.<sup>48–50</sup> The EPSR-generated trajectories were further interrogated to extract structural information on bulk ChAc:U.

Figure 3 shows the center of mass pair distribution functions (pdfs) for the three moieties in ChAc:U, namely, choline cation (C), acetate anion (A), and urea (U). It emerges that strong correlations exist between differently charged ionic species and between urea and all the components. Correlations between ionic species with the same charge are instead weaker and less well defined. CC correlations are characterized by a weak broad peak centered at  $\sim 6.5 \text{ \AA}$ ,

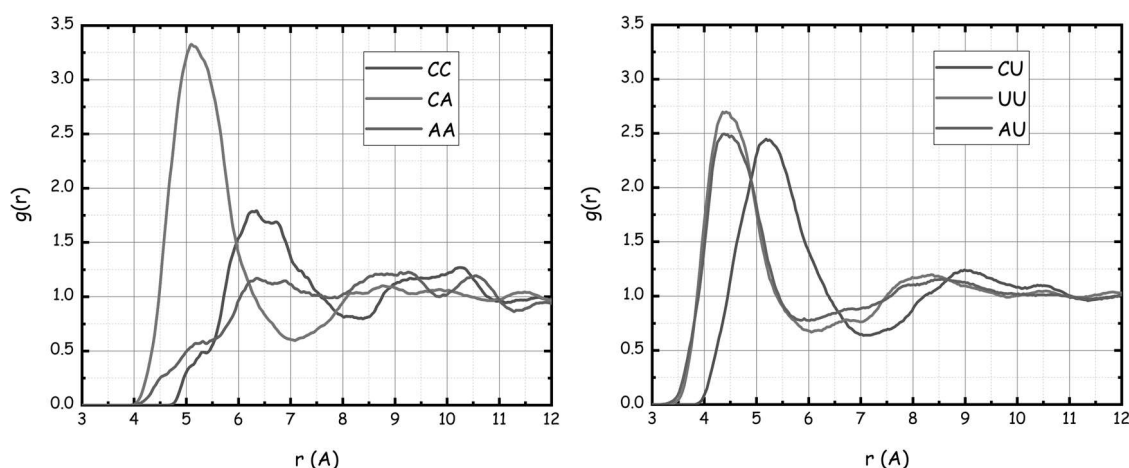


**FIG. 3.** Pair distribution function between centers of mass of ionic species [cation (C) and anion (A)] (left) and urea (U) with A and C (right) in ChAc:U, as obtained from EPSR modeling.

building up a solvation shell containing  $\sim 3$  moieties. This coordination number is substantially different from what is found in the case of reline, where choline is surrounded by approximately six other choline cations. Such a situation likely stems from the larger size, as well as the different shape and symmetry of acetate as compared to chloride anions. Each choline cation is on average surrounded by 3.4 acetate anions with a correlation peak at  $5.3 \text{ \AA}$ . For comparison in reline, 4.5 chloride anions were found in the first shell,<sup>10</sup> while one chloride anion was found in the same shell in malicine.<sup>51</sup> Urea is characterized by strong correlations both with other urea moieties and with cations and anions. First solvation shells are detected around each ionic species, with peaks centered at  $5.1$  and  $4.5 \text{ \AA}$  and six and four nearest neighbor urea moieties for choline and acetate, respectively.

Figure 4 reports a series of pdfs related to selected correlations between atomic species belonging to different moieties building up bulk ChAc:U.

The selected pdfs indicate the existence of strong correlations between the different moieties. In particular, those pdfs involving acetate and either choline or urea are characterized by strong peaks, fingerprinting hydrogen-bonding mediated interactions. Such interactions will further be explored later in this article. Choline–choline correlations are rather weak and broadly distributed. The strongest correlation is between neighbor nitrogen atoms, with a peak centered at  $6.5 \text{ \AA}$  and a neighbor number of  $\sim 2.5$  up to  $7 \text{ \AA}$ . We also detect a relatively strong N1–COH correlation centered at  $\sim 5.3 \text{ \AA}$  with  $\sim 2.5$  nearest neighbor (n.n.); however, there is only weak interaction of nitrogen with the hydroxyl group (weak peaks for N1–OH between  $4$  and  $5 \text{ \AA}$ ). Neighbor acetate anions are only correlated through their methyl groups for which we detect a C1x–C1x peak at  $4 \text{ \AA}$ , with one methyl group directly correlated with the reference one. Urea–urea correlations look more structured: we will later see that this is also because of the existence of hydrogen bonding interactions, and accordingly, we find a strong peak in the OU–NU pdf at  $\sim 3 \text{ \AA}$ , with a n.n. population of two NUs around the reference OU. The other peaks reported in Fig. 4(c) also indicate the existence of strong correlations between other moieties of urea, such as NU–NU

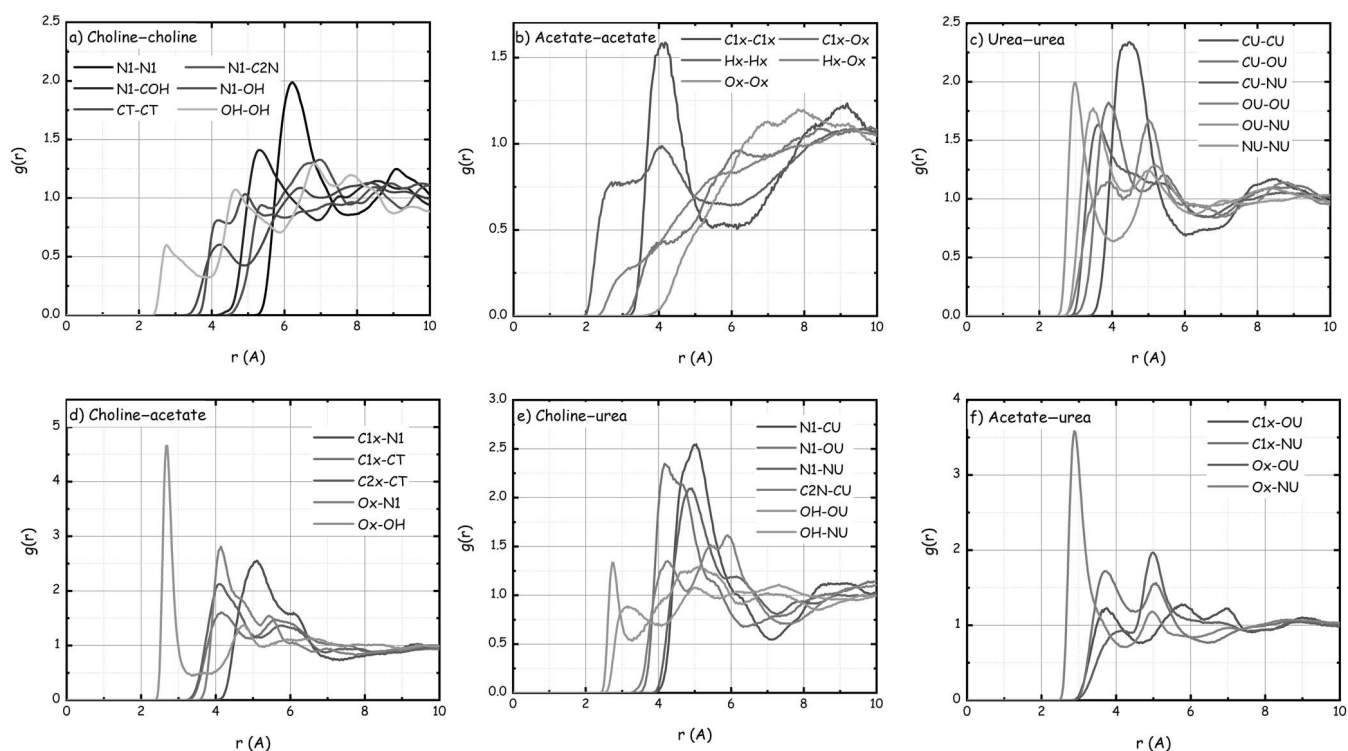


**FIG. 4.** Selected pair distribution functions between different atomic species belonging to the three moieties in ChAc:U (choline, acetate, and urea, respectively), after EPSR modeling.

(3 n.n.), CU-OU (2 n.n.) and, in particular, CU-CU (4 n.n.). Similar observations led Hammond *et al.* to propose the existence of urea clustering in reline.<sup>10</sup> Inter-species correlations are dominated, as we will see later in more detail, by HB correlations. Overall, these correlations look much stronger than correlations between similar species. The selected pdfs in Figs. 4(d)–4(f) reflect in an indirect way the existence of such interactions. Choline–acetate correlations are characterized by a strong Ox-OH peak at 2.7 Å, fingerprinting the HB between the two species. The broad peak related to the cation–anion pdf in Fig. 3 is likely related to the existence of different solvation scenarios of acetate around the reference choline: in particular, acetate will coordinate choline both at the hydroxyl side and at the ammonium side. This latter scenario is fingerprinted in the Ox-N1 and C1x-N1 pdfs by the strong peaks centered at 4.2 and 5 Å, respectively. Choline and urea appear to interact mostly through choline’s ammonium: pdf peaks for N1 with CU, NU, and OU are eminent at distances between 4 and 5.5 Å. Correlations mediated through choline’s hydroxyl group look weaker. The competition between acetate and urea in coordinating choline’s N1 leads to ~5 urea and three acetate moieties surrounding N1 by a distance of ~7 Å. For comparison, the OH moiety of choline is solvated with 0.6 acetate and 0.9 urea in the first shell (up to 4.5 Å) and ~2 choline in the first shell (up to 7 Å). Acetate and urea interact through HB involving urea’s hydrogen and the carboxyl group; such an interaction, fingerprinted by the Ox-NU peak at ca 3 Å, is consistent with two different solvation environments indicated by the two peaks in the C1x-NU pdf (3.7 and 5 Å).

As mentioned, HB interactions are fundamental in driving structural correlations in ChAc:U. In Fig. 5, the pair distribution functions associated with such correlations involve either the choline HOH or the urea HU1/2 donor groups. In particular, we specifically monitor the two hydrogens, HU1 and HU2, attached to the same nitrogen in urea (HU1 being the hydrogens in trans with the urea’s oxygen and HU2 being the cis-hydrogens), aiming at assessing differences in the HB features, due to steric hindrance. For these HB correlations, the combined distribution functions accounting for the distance  $H \cdots O$  and the angle  $D-H \cdots O$  (where D is the HB donor atom) are reported in the supplementary material (Figs. S1–S3). In all cases, HB involving the acetate HB acceptor (Ox) is characterized by the shortest and strongest interaction; in addition, the angular dependence of these HB reflects their linearity. In terms of pdf peak amplitude, the next most intense peaks correspond to those involving urea’s oxygen (OU) and finally choline’s oxygen (OH). Overall, all these HB interactions are found to be characterized by a quite linear geometry, as shown in Figs. S1–S3. In order to better illustrate the balance between HB donor and acceptor capabilities of the different moieties in ChAc:U, we exploit the linear Sankey diagram approach of Fig. 6, introduced recently for this kind of analysis.<sup>39</sup> A wealth of information can straightforwardly be extracted from such a plot, by the nature of HB networking in ChAc:U. The hydrogen bond donated by choline OH (HOH) (upper left) is mainly involved with acetate Ox (lower right). There is only a tiny amount of hydrogen bonding interaction between HOH and choline OH and negligible interaction with urea. The trans- and cis-protons of urea (HU1

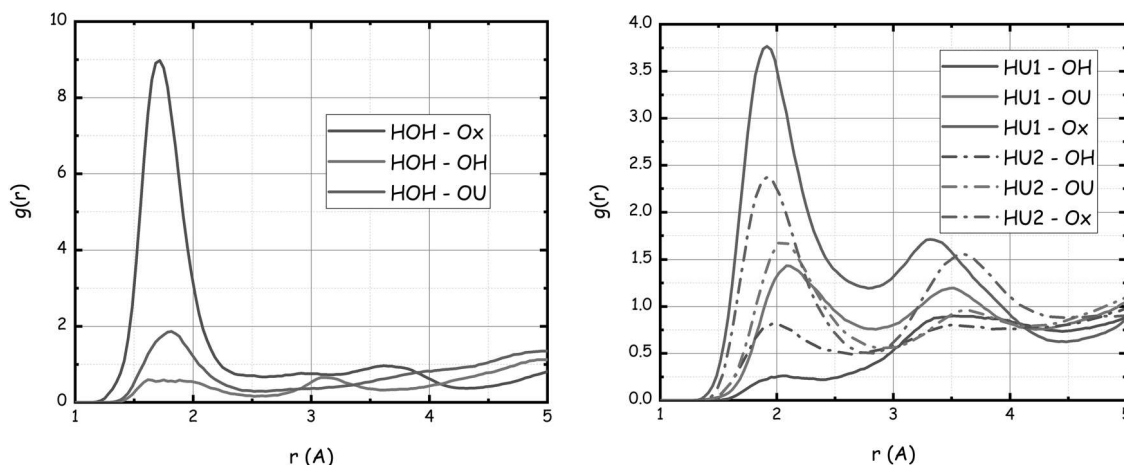


**FIG. 5.** Pair distribution functions related to hydrogen bonding interactions in ChAc:U, as obtained from the EPSR modeling: (left) pdf related to the HOH donor agent in choline and (right) pdf related to the trans (HU1) and cis (HU2) hydrogens in urea.

and HU2, respectively) behave differently. While the trans-protons (HU1, middle left) do not form hydrogen bonds with choline OH but form strong hydrogen bonds with both urea OU and acetate Ox, the cis protons (HU2, lower left) also form hydrogen bonds with choline OH. Now, considering the acceptors (right side), incoming hydrogen bonds at choline OH almost exclusively come from the urea cis-protons, HU2. The urea oxygen receives strong hydrogen bonds from both cis- and trans-protons of urea, while it almost receives no hydrogen bonds from choline HOH. A similar picture arises for acetate Ox, where the hydrogen bond received from the urea trans-protons is most significant. Overall, the major role played by the acetate anion in establishing HB interactions is confirmed

by this graph; analogously, the minor role played by choline's OH acceptor site is also highlighted.

Additional understanding of the mutual spatial distribution of the different species with respect to each other can be obtained by inspecting the spatial distribution functions reported in Fig. 7. The first of such plots refers to the distribution of the three different moieties surrounding a reference urea molecule. Urea is strongly correlated with acetate anions (red lobes) at spatial locations corresponding to its cis- and trans-hydrogens. Choline cations (blue lobes) distribute in a much more homogeneous way around urea, and correlations are not driven by HB, but rather by dispersive interactions. Finally, urea (yellow lobes) competes with acetate to access the reference urea hydrogens; it moreover interacts with reference urea oxygen. It also appears that choline tends to distribute around urea, also aiming at interacting with the other species surrounding the reference one. In Fig. 7, the distributions around a reference choline cation are also shown. The acetate anion is strongly interacting with the hydroxyl group, with a weak competition on this site with urea; otherwise, both the choline cation and urea are distributed rather homogeneously around the whole reference choline, with urea approaching closer than choline the reference molecule. Figure 7 also shows the distributions of cations and urea around a reference acetate anion. The two species have similar distributions, although urea succeeds in accessing closer to the anion, presumably due to its smaller size. Both moieties approach the anion from the charged carboxyl part, thus reflecting the development of hydrogen bonding interactions. Anions tend to approach the reference acetate from the opposite side, leading to methyl–methyl group correlations (data not shown).

These pictures are consistent with the overwhelming role played by acetate in HB interacting with both urea's and choline's HB donor hydrogens. On the other hand, the HB donor and acceptor nature of urea and the possibility of choline to interact not only with Coulombic forces but also with dispersive ones make these two moieties able to efficiently solvate any component in ChAc:U. Analogously to the case of reline, an intertwining of the different species

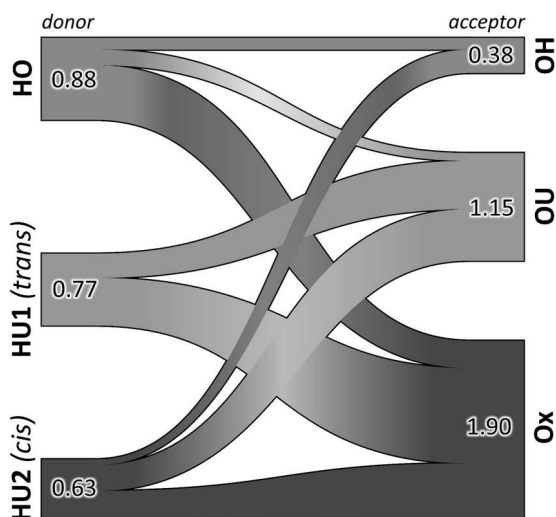


**FIG. 6.** Linear Sankey diagram describing the hydrogen bonding topology in ChAc:U. Numbers correspond to the average hydrogen bond count per donor/acceptor.

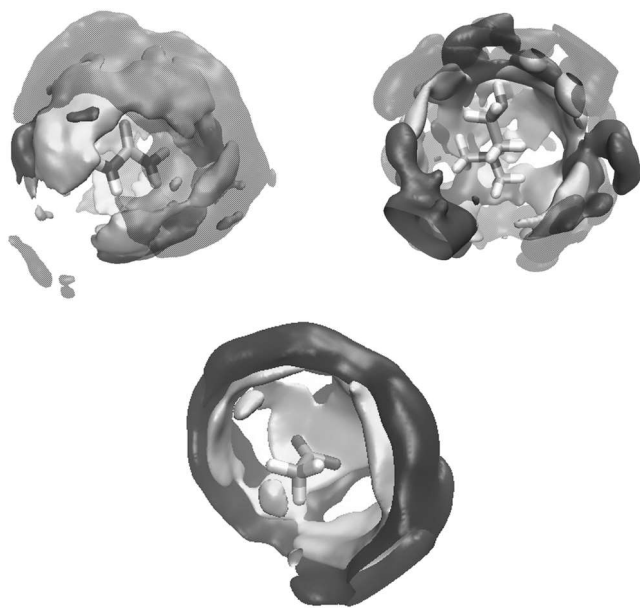


**FIG. 7.** Spatial distribution functions around reference urea (top, left), choline (top, right), and acetate (bottom, left). The colored lobes correspond to 20% distribution of choline (blue), acetate (red), and urea (yellow) in ChAc:U.

occurs in delivering an intimate mixing of these components at the atomic level.

To corroborate the structural picture emerging from the combined x-ray/reverse Monte Carlo approach, variable-temperature NMR measurements were performed. As inter-species correlations appear to be dominated by HB interactions, the upfield or downfield movement of the temperature-dependent  $^1\text{H}$  chemical shift was monitored to give a preliminary insight into the strength of the HB of the detected proton. Figure 8 shows the relative shifts of the  $^1\text{H}$  NMR signals of ChAc:U, which are defined as  $\Delta\delta = \delta - \delta_0$ , with  $\delta_0$  being the chemical shift of a given proton in the pure DES and  $\delta$  being the chemical shift of the same proton for increased temperature.<sup>52,53</sup> The remarkable upfield shift of urea protons is compatible with a weakening of the H-bond strength at the urea site with temperature<sup>54</sup> and points toward their strong involvement in the HB network of the mixture. No relevant changes are observed for the choline signals, including the N-methyl groups, which are in line with a minor role played by the cation in the intermolecular network. Only a tiny upfield shift emerges for the methyl group of acetate, as they do not directly participate in the HB interactions but most likely feel a pale indirect effect of the major role played by the acidic group of the anion.

The NMR experiments of choice to probe spatial intermolecular networks are typically based on the nuclear Overhauser enhancement (NOE). In extensively connected systems such as DES, it is, however, quite common to observe intra- and inter-correlations between all sites/species in the mixtures.<sup>55,56</sup> This is the case for ChAc:U too, as displayed in Fig. S4 of the supplementary material. Due to spin diffusion and/or exchange (facilitated by the residual water), all signals are positive. Choline shows intramolecular NOE signals, and intermolecular NOEs are observed between all the three

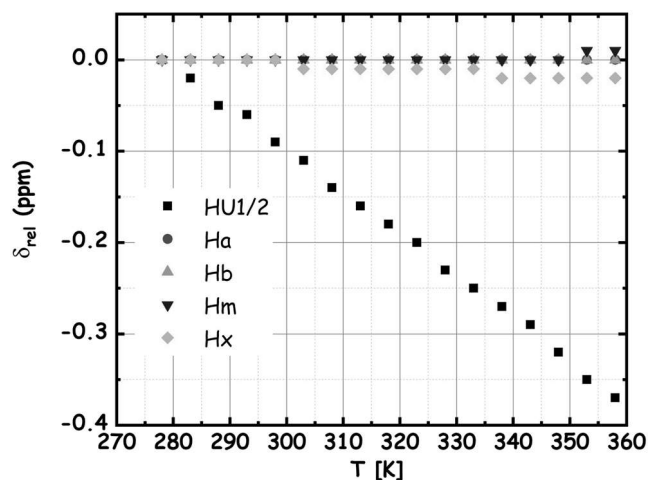


**FIG. 8.**  $^1\text{H}$  relative shift observed for ChAc:U as a function of temperature.

species: choline, acetate, and urea. As expected, intense correlations are observed between the hydroxyl group proton of choline and urea and the N-methyl groups of choline and urea. The methyl group of acetate shows the strongest correlations with the N-methyl protons of choline and with urea. This confirms the major role of these protons in the interactions, holding the DES components together.

The NOESY data then provide support to the scenario of an extended HB network in the DES, which is the root of its peculiar macroscopic properties. We also exploited relaxation and diffusion NMR experiments to shed more light on the system. Intermolecular interactions and dynamics are, indeed, intertwined as strong correlations reduce motion—as one can intuitively envisage.  $T_1$  relaxation times and self-diffusion coefficients were measured over an 80 °C temperature interval and analyzed to get quantitative descriptors of the motion(s).

As displayed in Fig. S5 of the supplementary material, all temperature-dependent  $T_1$  curves, but that corresponding to methyl protons of acetate, pass through a minimum. This indicates that the protons of choline and urea undergo a transition from the extreme narrowing ( $\omega_0\tau_C < 1$ ) to the diffusion limit ( $\omega_0\tau_C > 1$ ) relaxation regime between  $\sim 25$  and  $\sim 50$  °C. Contrarily, the methyl protons of the anion fail to undergo this transition in the studied temperature range due to their higher mobility. In the case of  $^1\text{H}$   $T_1$ , where the predominant relaxation mechanism is the homonuclear dipole-dipole interaction, the relaxation rate  $R_1$  is defined by the Bloembergen, Purcell, and Pound (BPP) approach as<sup>57–59</sup>

$$R_1 = \frac{1}{T_1} = C \left( \frac{\tau_C}{1 + \omega_0^2\tau_C^2} + \frac{4\tau_C}{1 + 4\omega_0^2\tau_C^2} \right), \quad (1)$$

with  $\omega_0$  being the observe frequency ( $\text{rad s}^{-1}$ ) and  $C$  being a term evaluated separately for each nucleus. The correlation time of the dipolar interaction  $\tau_C$  can be thought of as the time required for the vector connecting the interacting nuclei to rotate through the angle of one radian, and for small rigid molecules, it commonly reflects the molecular reorientational time constant.<sup>59</sup> As for flexible ionic liquids,<sup>60,61</sup>  $\tau_C$  observed for ChAc:U have to be rather considered



as a combination of molecular reorientation and internal motions of each given segment. From the term in brackets in Eq. (1), it follows that  $T_1$  is minimum when  $\omega_0\tau_C = 2\pi\nu_0\tau_C = 0.616$ ,<sup>61–63</sup> which here means that  $\tau_C = 0.616/(2\pi \cdot 500.13 \cdot 10^6 \text{ Hz}) = 196 \text{ ps}$ . Such a minimum  $T_1$  value can be used to calculate  $C$  from Eq. (1), then enabling the calculations of  $\tau_C$  values from the  $T_1$  values observed at any temperature. The temperature-dependent correlation times can then be used in an Arrhenius-type equation to calculate the “apparent” activation energy  $E_a^{\text{rot}}$  (averaged over several types of movements).<sup>61,64</sup> Alternatively, by substituting the function of the correlation time approximated as an Arrhenius expression into the BPP equation [Eq. (1)] and assuming  $C$  temperature insensitive, the combined equation can directly be solved, yielding the same outputs within the experimental error.<sup>61,65</sup> Although the two methods are essentially the same from the theoretical standpoint, the latter nonlinear least-squares method is useful in cases where an exact minimum is not reached in the examined temperature range and is recommended even for protons where a  $T_1$  minimum can be distinctly observed as it needs less steps with a reduced margin of error.<sup>61</sup> The nonlinear least-squares method was used here to fit all  $T_1$  data, obtaining the correlation times and activation energies reported in Fig. 9. All temperature-dependent curves perfectly followed the BPP model, which means that a single basic motion occurs in the studied temperature range.<sup>62</sup> The best-fit parameters are given in Table S1 of the supplementary material, together with those obtained by applying the most widely used method based on the  $T_1$  minimum followed by the Arrhenius plot of the activation energies, to confirm that comparable results are obtained. Urea protons show the longest  $\tau_C$  values (slowest rotational motion) and the methyl protons of acetate the shortest ones (fastest rotational motion), while the three methylene and methyl sites of choline exhibited all close, intermediate  $\tau_C$  values. A direct comparison between the correlation times of the different sites and species is complicated due to the contribution of different relaxation mechanisms. More informative are the rotational activation energies, which mark a significant difference between acetate from the one side, with  $E_a^{\text{rot}}$  of  $\sim 12 \text{ kJ mol}^{-1}$ , and choline and urea from the other, all with  $E_a^{\text{rot}}$  above  $20 \text{ kJ mol}^{-1}$ . Hence,

the rotational motion of the acetate protons is not only the fastest, also due to the intramolecular rotation around the symmetry axis of the methyl group, but it also requires less energy to occur. For the sake of completeness, we also report the correlation times and rotational activation energy obtained from the BPP analysis of the temperature-dependent  $T_1$  data of the peak corresponding to the residual water and the hydroxyl proton of choline (Fig. S5 and Fig. 9). All  $T_1$ ,  $\tau_C$ , and  $E_a^{\text{rot}}$  values essentially overlap those corresponding to urea protons, pointing toward a strong correlation between the rotational motions of the two species. Despite its relevance, the role of water in the intermolecular network of ChAc:U is beyond the scope of the present paper and will be deepened in a separate work on hydrated ChAc:U. Here, the focus is on the role of the DES constituents—choline, acetate, and urea—and we can safely assume that the residual water molecules will participate in the intermolecular network without drastic alterations of the mutual relationships among them.

In order to monitor the translational mobility and gather a more complete overview of the system, the self-diffusion coefficients of the different ChAc:U moieties were measured by PFG NMR. The diffusivities,  $D$ , probed in the range of 278–358 K are given in Fig. S6 and Table S2 of the supplementary material. As expected, the diffusion coefficients measured for the methylene protons of choline yielded the same value as  $\text{CH}_3$ ; hence, only the latter is presented. The temperature dependence of the diffusion coefficients over the whole probed temperature range was modeled in terms of an Arrhenius-activated process. Translational activation energies are reported in Fig. 10, and fit parameters are presented in Table S3 of the supplementary material. While the activation energies associated with relaxation data are in the range of 10–30  $\text{kJ mol}^{-1}$ , the activation energies associated with diffusion data are larger (40–50  $\text{kJ mol}^{-1}$ ). This is due to the different molecular motion, affecting these apparent activation energies, rotational vs translational, and is in agreement with behaviors found, for instance, in ionic liquids.<sup>66,67</sup> Noteworthy is the order of  $E_a^{\text{transl}}$ : urea  $\approx \text{H}_2\text{O} + \text{OH} > \text{acetate} > \text{choline}$ . This is unrelated to the molecular size of the species and can only be explained by admitting that the translational motion of urea and acetate is slowed down by their

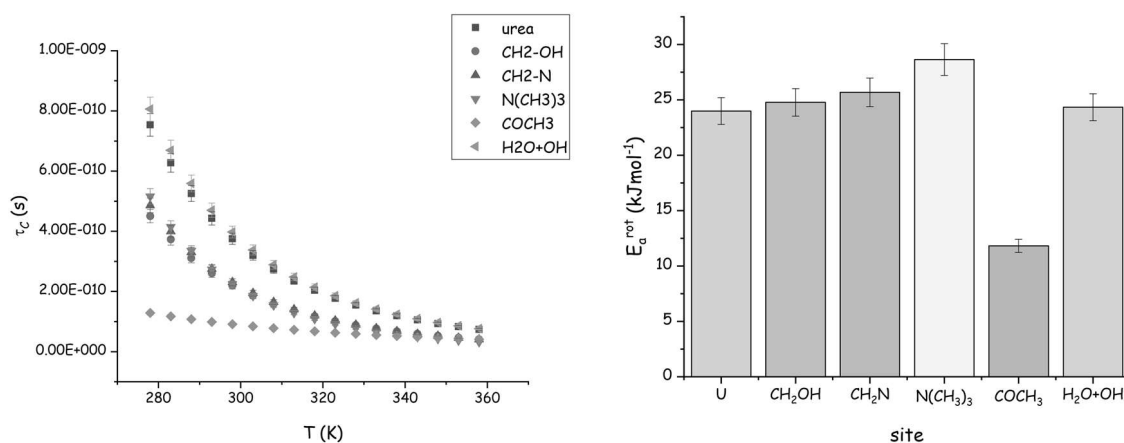


FIG. 9. (left)  $^1\text{H}$  correlation times  $\tau_C$  vs temperature and (right) rotational activation energy  $E_a^{\text{rot}}$  ( $\text{kJ mol}^{-1}$ ) obtained for the different proton sites of ChAc:U.

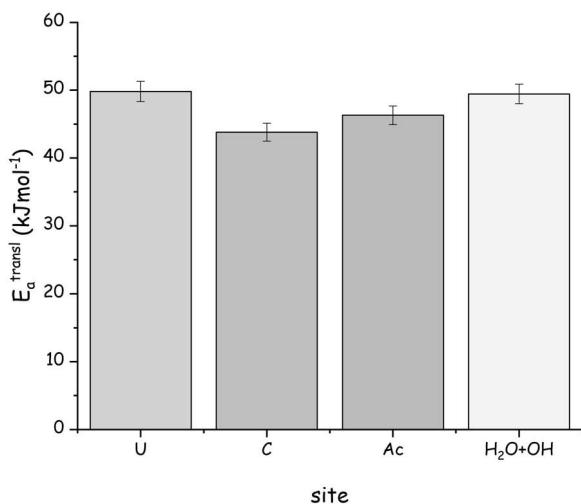


FIG. 10. Translational activation energy  $E_a^{\text{transl}}$  (kJ mol<sup>-1</sup>) obtained for all species in ChAc:U.

strong involvement in the HB network. The major role of urea and acetate in the intermolecular network, inferred here from a dynamic parameter, fits the molecular picture outlined by means of more common techniques for structure elucidation, such as x ray and NOESY. Note, also, that this prominent role is maintained here even in the presence of residual amounts of water (5.7 wt. %). Contrarily, the activation energy of choline is the lowest one, regardless of its higher size due to its less fundamental role in the intermolecular connections. As urea has proven to strongly connect with other constituents in several DESs using both the oxygen and proton nuclei (see also the linear Sankey diagram in Fig. 6), its reduced rotational and translational mobilities (high  $E_a^{\text{rot}}$  and  $E_a^{\text{transl}}$ ) are quite expected. The peculiar role of acetate is, instead, not a foregone conclusion. The key role of this small anion in the HB network keeps it on a tight leash, strongly affecting its translational mobility and increasing its  $E_a^{\text{transl}}$ , which is a dynamic indicator of the whole molecule. Contrarily, the rotational mobility of the methyl protons of acetate does not suffer from a strong effect as they are not directly participating in the HB network. Hence, the corresponding  $E_a^{\text{rot}}$ —a local dynamic parameter—is still smaller than the rotational activation energy of all other proton sites of both choline and urea.

## CONCLUSION

Choline acetate mixtures with urea at a stoichiometric composition of 1:2 are deep eutectic media whose melting point is  $\sim 40^\circ\text{C}$ , but it can easily be supercooled into the liquid state at sub-ambient conditions. The liquid ChAc:U structure at the atomistic level has been investigated by means of synchrotron high energy x-ray diffraction, supported by the EPSR Reverse Monte Carlo analysis approach that allows for extracting detailed information on the mutual interactions between moieties of ChAc:U. Hydrogen bonding plays a major role in determining structure in liquid ChAc:U. Radial distribution functions show how acetate-mediated HBs are among the strongest in the system; urea also plays a major role as the HB donor, and these correlations are straightforwardly described by the use of

a Sankey diagram, illustrating HB flow among the different donor and acceptor moieties. A complex intertwining of different moieties is observed with Coulombic interactions (via HB correlations) mostly involving acetate and urea, while choline is mostly involved in dispersive interactions. This peculiar situation is mirrored in the dynamics monitored in ChAc:U. While acetate's methyl group shows the lowest correlation times and activation energy considering <sup>1</sup>H rotational motion, the anion diffuses slower than expected from its size, thus confirming its strong role in the HB network. Choline turns out to be the moiety with the lowest activation energy concerning diffusive dynamics, reflecting its secondary involvement into the HB interaction network.

## SUPPLEMENTARY MATERIAL

See the supplementary material for combined distribution functions accounting for the hydrogen bonding geometries, NMR plots and tables, and EPSR force field parameters.

## ACKNOWLEDGMENTS

This work was supported by the University of Rome Sapienza Projects: “Microscopic and mesoscopic organization in ionic liquid-based systems” (Grant No. RG11715C7CC660BE) and “Green solvents for simple and complex carbohydrates” (Grant No. RM120172B2165468).

M.B. acknowledges financial support from the Deutsche Forschungsgemeinschaft (DFG) through Project No. Br 5494/1-1.

M.E.D.P. thanks Politecnico di Milano for her postdoctoral fellowship in the framework of the “MSCA EF Master Class 2018” funding program.

Access to Professor S. Brutti's laboratories (Univ. Rome—Sapienza) is gratefully acknowledged.

We thank Diamond Light Source for access to beamline I15-1 (Grant No. CY27222-1) that contributed to the results presented here.

## DATA AVAILABILITY

The data that support the findings of this study are available from the corresponding authors upon reasonable request.

## REFERENCES

- <sup>1</sup>A. P. Abbott, G. Capper, D. L. Davies, R. K. Rasheed, and V. Tambyrajah, “Novel solvent properties of choline chloride/urea mixtures,” *Chem. Commun.* **2003**(1), 70–71.
- <sup>2</sup>A. P. Abbott, D. Boothby, G. Capper, D. L. Davies, and R. K. Rasheed, “Deep eutectic solvents formed between choline chloride and carboxylic acids: Versatile alternatives to ionic liquids,” *J. Am. Chem. Soc.* **126**(29), 9142–9147 (2004).
- <sup>3</sup>E. L. Smith, A. P. Abbott, and K. S. Ryder, “Deep eutectic solvents (DESs) and their applications,” *Chem. Rev.* **114**(21), 11060–11082 (2014).
- <sup>4</sup>D. V. Wagle, H. Zhao, and G. A. Baker, “Deep eutectic solvents: Sustainable media for nanoscale and functional materials,” *Acc. Chem. Res.* **47**(8), 2299–2308 (2014).
- <sup>5</sup>Q. Zhang, K. De Oliveira Vigier, S. Royer, and F. Jérôme, “Deep eutectic solvents: Syntheses, properties and applications,” *Chem. Soc. Rev.* **41**(21), 7108–7146 (2012).
- <sup>6</sup>A. Paiva, R. Craveiro, I. Aroso, M. Martins, R. L. Reis, and A. R. C. Duarte, “Natural deep eutectic solvents—Solvents for the 21st century,” *ACS Sustainable Chem. Eng.* **2**(5), 1063–1071 (2014).

- <sup>7</sup>A. Roda, A. Matias, A. Paiva, and A. Duarte, "Polymer science and engineering using deep eutectic solvents," *Polymers* **11**(5), 912 (2019).
- <sup>8</sup>F. M. Perna, P. Vitale, and V. Capriati, "Deep eutectic solvents and their applications as green solvents," *Curr. Opin. Green Sustainable Chem.* **21**, 27–33 (2020).
- <sup>9</sup>S. L. Perkins, P. Painter, and C. M. Colina, "Molecular dynamic simulations and vibrational analysis of an ionic liquid analogue," *J. Phys. Chem. B* **117**(35), 10250–10260 (2013).
- <sup>10</sup>O. S. Hammond, D. T. Bowron, and K. J. Edler, "Liquid structure of the choline chloride-urea deep eutectic solvent (reline) from neutron diffraction and atomistic modelling," *Green Chem.* **18**(9), 2736–2744 (2016).
- <sup>11</sup>M. Gilmore, L. M. Moura, A. H. Turner, M. Swadźba-Kwaśny, S. K. Callear, J. A. McCune, O. A. Scherman, and J. D. Holbrey, "A comparison of choline:urea and choline:oxalic acid deep eutectic solvents at 338 K," *J. Chem. Phys.* **148**(19), 193823 (2018).
- <sup>12</sup>E. O. Fetisov, D. B. Harwood, I.-F. W. Kuo, S. E. E. Warrag, M. C. Kroon, C. J. Peters, and J. I. Siepmann, "First-principles molecular dynamics study of a deep eutectic solvent: Choline chloride/urea and its mixture with water," *J. Phys. Chem. B* **122**(3), 1245–1254 (2018).
- <sup>13</sup>C. F. Araujo, J. A. P. Coutinho, M. M. Nolasco, S. F. Parker, P. J. A. Ribeiro-Claro, S. Rudić, B. I. G. Soares, and P. D. Vaz, "Inelastic neutron scattering study of reline: Shedding light on the hydrogen bonding network of deep eutectic solvents," *Phys. Chem. Chem. Phys.* **19**(27), 17998–18009 (2017).
- <sup>14</sup>C. R. Ashworth, R. P. Matthews, T. Welton, and P. A. Hunt, "Doubly ionic hydrogen bond interactions within the choline chloride-urea deep eutectic solvent," *Phys. Chem. Chem. Phys.* **18**(27), 18145–18160 (2016).
- <sup>15</sup>A. Triolo, F. Lo Celso, and O. Russina, "Structural features of  $\beta$ -cyclodextrin solvation in the deep eutectic solvent, reline," *J. Phys. Chem. B* **124**(13), 2652–2660 (2020).
- <sup>16</sup>M. E. Di Pietro, O. Hammond, A. van den Bruinhorst, A. Mannu, A. Padua, A. Mele, and M. Costa Gomes, "Connecting chloride solvation with hydration in deep eutectic systems," *Phys. Chem. Chem. Phys.* **23**(1), 107–111 (2021).
- <sup>17</sup>M. Gilmore, M. Swadźba-Kwaśny, and J. D. Holbrey, "Thermal properties of choline chloride/urea system studied under moisture-free atmosphere," *J. Chem. Eng. Data* **64**(12), 5248–5255 (2019).
- <sup>18</sup>F. Gabriele, M. Chiarini, R. Germani, M. Tiecco, and N. Spreti, "Effect of water addition on choline chloride/glycol deep eutectic solvents: Characterization of their structural and physicochemical properties," *J. Mol. Liq.* **291**, 111301 (2019).
- <sup>19</sup>D. V. Wagle, G. A. Baker, and E. Mamontov, "Differential microscopic mobility of components within a deep eutectic solvent," *J. Phys. Chem. Lett.* **6**(15), 2924–2928 (2015).
- <sup>20</sup>R. Stefanovic, M. Ludwig, G. B. Webber, R. Atkin, and A. J. Page, "Nanostructure, hydrogen bonding and rheology in choline chloride deep eutectic solvents as a function of the hydrogen bond donor," *Phys. Chem. Chem. Phys.* **19**(4), 3297–3306 (2017).
- <sup>21</sup>A. H. Turner and J. D. Holbrey, "Investigation of glycerol hydrogen-bonding networks in choline chloride/glycerol eutectic-forming liquids using neutron diffraction," *Phys. Chem. Chem. Phys.* **21**(39), 21782–21789 (2019).
- <sup>22</sup>S. L. Perkins, P. Painter, and C. M. Colina, "Experimental and computational studies of choline chloride-based deep eutectic solvents," *J. Chem. Eng. Data* **59**(11), 3652–3662 (2014).
- <sup>23</sup>S. Kaur, A. Malik, and H. K. Kashyap, "Anatomy of microscopic structure of ethaline deep eutectic solvent decoded through molecular dynamics simulations," *J. Phys. Chem. B* **123**(39), 8291–8299 (2019).
- <sup>24</sup>Y. Zhang, D. Poe, L. Heroux, H. Squire, B. W. Doherty, Z. Long, M. Dadmun, B. Gurkan, M. E. Tuckerman, and E. J. Maginn, "Liquid structure and transport properties of the deep eutectic solvent ethaline," *J. Phys. Chem. B* **124**(25), 5251–5264 (2020).
- <sup>25</sup>H. Zhang, M. L. Ferrer, M. J. Roldán-Ruiz, R. J. Jiménez-Riobóo, M. C. Gutiérrez, and F. Del Monte, "Brillouin spectroscopy as a suitable technique for the determination of the eutectic composition in mixtures of choline chloride and water," *J. Phys. Chem. B* **124**(19), 4002–4009 (2020).
- <sup>26</sup>M. S. Rahman and D. E. Raynie, "Thermal behavior, solvatochromic parameters, and metal halide solvation of the novel water-based deep eutectic solvents," *J. Mol. Liq.* **324**, 114779 (2020).
- <sup>27</sup>A. Triolo, F. Lo Celso, M. Brehm, V. Di Lisio, and O. Russina, "Liquid structure of a choline chloride-water natural deep eutectic solvent: A molecular dynamics characterization," *J. Mol. Liq.* **331**, 115750 (2021).
- <sup>28</sup>Y. Fukaya, Y. Iizuka, K. Sekikawa, and H. Ohno, "Bio ionic liquids: Room temperature ionic liquids composed wholly of biomaterials," *Green Chem.* **9**(11), 1155–1157 (2007).
- <sup>29</sup>H. Zhao, G. A. Baker, and S. Holmes, "New eutectic ionic liquids for lipase activation and enzymatic preparation of biodiesel," *Org. Biomol. Chem.* **9**(6), 1908–1916 (2011).
- <sup>30</sup>J. Hoppe, R. Drozd, E. Byzia, and M. Smiglak, "Deep eutectic solvents based on choline cation—Physicochemical properties and influence on enzymatic reaction with  $\beta$ -galactosidase," *Int. J. Biol. Macromol.* **136**, 296–304 (2019).
- <sup>31</sup>G. Colombo Dugoni, A. Mezzetta, L. Guazzelli, C. Chiappe, M. Ferro, and A. Mele, "Purification of kraft cellulose under mild conditions using choline acetate based deep eutectic solvents," *Green Chem.* **22**, 8680–8691 (2020).
- <sup>32</sup>J. Filik, A. W. Ashton, P. C. Y. Chang, P. A. Chater, S. J. Day, M. Drakopoulos, M. W. Gerring, M. L. Hart, O. V. Magdysyuk, S. Michalik, A. Smith, C. C. Tang, N. J. Terrill, M. T. Wharmby, and H. Wilhelm, "Processing two-dimensional X-ray diffraction and small-angle scattering data in DAWN2," *J. Appl. Crystallogr.* **50**(3), 959–966 (2017).
- <sup>33</sup>A. K. Soper and E. R. Barney, "Extracting the pair distribution function from white-beam X-ray total scattering data," *J. Appl. Crystallogr.* **44**(4), 714–726 (2011).
- <sup>34</sup>A. K. Soper, "The radial distribution functions of water as derived from radiation total scattering experiments: Is there anything we can say for sure?," *ISRN Phys. Chem.* **2013**, 1–67.
- <sup>35</sup>A. K. Soper, "Empirical potential Monte Carlo simulation of fluid structure," *Chem. Phys.* **202**(2-3), 295–306 (1996).
- <sup>36</sup>A. K. Soper, E. W. Castner, and A. Luzar, "Impact of urea on water structure: A clue to its properties as a denaturant?," *Biophys. Chem.* **105**(2-3), 649–666 (2003).
- <sup>37</sup>D. T. Bowron, C. D'Agostino, L. F. Gladden, C. Hardacre, J. D. Holbrey, M. C. Lagunas, J. McGregor, M. D. Mantle, C. L. Mullan, and T. G. A. Youngs, "Structure and dynamics of 1-ethyl-3-methylimidazolium acetate via molecular dynamics and neutron diffraction," *J. Phys. Chem. B* **114**(23), 7760–7768 (2010).
- <sup>38</sup>M. Brehm and B. Kirchner, "TRAVIS—A free analyzer and visualizer for Monte Carlo and molecular dynamics trajectories," *J. Chem. Inf. Model.* **51**(8), 2007–2023 (2011).
- <sup>39</sup>M. Brehm, M. Thomas, S. Gehrke, and B. Kirchner, "TRAVIS—A free analyzer for trajectories from molecular simulation," *J. Chem. Phys.* **152**(16), 164105 (2020).
- <sup>40</sup>O. Hollóczy, M. Macchiagodena, H. Weber, M. Thomas, M. Brehm, A. Stark, O. Russina, A. Triolo, and B. Kirchner, "Triphasic ionic-liquid mixtures: Fluorinated and non-fluorinated aprotic ionic-liquid mixtures," *ChemPhysChem* **16**(15), 3325–3333 (2015).
- <sup>41</sup>S. Kaur, S. Sharma, and H. K. Kashyap, "Bulk and interfacial structures of reline deep eutectic solvent: A molecular dynamics study," *J. Chem. Phys.* **147**(19), 194507 (2017).
- <sup>42</sup>P. Kumari, Shobhna, S. Kaur, and H. K. Kashyap, "Influence of hydration on the structure of reline deep eutectic solvent: A molecular dynamics study," *ACS Omega* **3**(11), 15246–15255 (2018).
- <sup>43</sup>O. S. Hammond, D. T. Bowron, and K. J. Edler, "The effect of water upon deep eutectic solvent nanostructure: An unusual transition from ionic mixture to aqueous solution," *Angew. Chem., Int. Ed.* **56**(33), 9782–9785 (2017).
- <sup>44</sup>S. McDonald, T. Murphy, S. Imberti, G. G. Warr, and R. Atkin, "Amphiphilically nanostructured deep eutectic solvents," *J. Phys. Chem. Lett.* **9**(14), 3922–3927 (2018).
- <sup>45</sup>A. Triolo, O. Russina, H.-J. Bleif, and E. Di Cola, "Nanoscale segregation in room temperature ionic liquids," *J. Phys. Chem. B* **111**(18), 4641–4644 (2007).
- <sup>46</sup>O. Russina, A. Triolo, L. Gontrani, and R. Caminiti, "Mesoscopic structural heterogeneities in room-temperature ionic liquids," *J. Phys. Chem. Lett.* **3**(1), 27–33 (2012).
- <sup>47</sup>M. Macchiagodena, F. Ramondo, A. Triolo, L. Gontrani, and R. Caminiti, "Liquid structure of 1-ethyl-3-methylimidazolium alkyl sulfates by X-ray scattering and molecular dynamics," *J. Phys. Chem. B* **116**(45), 13448–13458 (2012).

- <sup>48</sup>O. Russina, A. Sferrazza, R. Caminiti, and A. Triolo, "Amphiphile meets amphiphile: Beyond the polar-apolar dualism in ionic liquid/alcohol mixtures," *J. Phys. Chem. Lett.* **5**(10), 1738–1742 (2014).
- <sup>49</sup>W. Schroer, A. Triolo, and O. Russina, "Nature of mesoscopic organization in protic ionic liquid-alcohol mixtures," *J. Phys. Chem. B* **120**(9), 2638–2643 (2016).
- <sup>50</sup>O. Russina, F. Lo Celso, N. V. Plechkova, and A. Triolo, "Emerging evidences of mesoscopic-scale complexity in neat ionic liquids and their mixtures," *J. Phys. Chem. B* **121**(31), 7473–7483 (2017).
- <sup>51</sup>O. S. Hammond, D. T. Bowron, A. J. Jackson, T. Arnold, A. Sanchez-Fernandez, N. Tsapatsaris, V. Garcia Sakai, and K. J. Edler, "Resilience of malic acid natural deep eutectic solvent nanostructure to solidification and hydration," *J. Phys. Chem. B* **121**(31), 7473–7483 (2017).
- <sup>52</sup>E. Posada, M. J. Roldán-Ruiz, R. J. Jiménez Riobóo, M. C. Gutiérrez, M. L. Ferrer, and F. del Monte, "Nanophase separation in aqueous dilutions of a ternary DES as revealed by Brillouin and NMR spectroscopy," *J. Mol. Liq.* **276**, 196–203 (2019).
- <sup>53</sup>C. A. Hall, K. A. Le, C. Rudaz, A. Radhi, C. S. Lovell, R. A. Damion, T. Budtova, and M. E. Ries, "Macroscopic and microscopic study of 1-ethyl-3-methyl-imidazolium acetate-water mixtures," *J. Phys. Chem. B* **116**(42), 12810–12818 (2012).
- <sup>54</sup>S. Grzesiek and E. D. Becker, "Hydrogen bonding," in *Encyclopedia of Magnetic Resonance* (John Wiley & Sons, Ltd., Chichester, UK, 2011).
- <sup>55</sup>R. Häkkinen, O. Alshammari, V. Timmermann, C. D'Agostino, and A. Abbott, "Nanoscale clustering of alcoholic solutes in deep eutectic solvents studied by nuclear magnetic resonance and dynamic light scattering," *ACS Sustainable Chem. Eng.* **7**(17), 15086–15092 (2019).
- <sup>56</sup>I. Delso, C. Lafuente, J. Muñoz-Embid, and M. Artal, "NMR study of choline chloride-based deep eutectic solvents," *J. Mol. Liq.* **290**, 111236 (2019).
- <sup>57</sup>N. Bloembergen, E. M. Purcell, and R. V. Pound, "Relaxation effects in nuclear magnetic resonance absorption," *Phys. Rev.* **73**(7), 679–712 (1948).
- <sup>58</sup>K. Hayamizu, S. Tsuzuki, S. Seki, and Y. Umebayashi, "Nuclear magnetic resonance studies on the rotational and translational motions of ionic liquids composed of 1-ethyl-3-methylimidazolium cation and bis(trifluoromethanesulfonyl)amide and bis(fluorosulfonyl)amide anions and their binary systems including Li," *J. Chem. Phys.* **135**(8), 084505 (2011).
- <sup>59</sup>K. Hayamizu, S. Tsuzuki, S. Seki, and Y. Umebayashi, "Multinuclear NMR studies on translational and rotational motion for two ionic liquids composed of BF<sub>4</sub> anion," *J. Phys. Chem. B* **116**(36), 11284–11291 (2012).
- <sup>60</sup>T. M. Alam, D. R. Dreyer, C. W. Bielwaski, and R. S. Ruoff, "Measuring molecular dynamics and activation energies for quaternary acyclic ammonium and cyclic pyrrolidinium ionic liquids using <sup>14</sup>N NMR spectroscopy," *J. Phys. Chem. A* **115**(17), 4307–4316 (2011).
- <sup>61</sup>M. E. Di Pietro, F. Castiglione, and A. Mele, "Polar/apolar domains' dynamics in alkylimidazolium ionic liquids unveiled by the dual receiver NMR <sup>1</sup>H and <sup>19</sup>F relaxation experiment," *J. Mol. Liq.* **322**, 114567 (2021).
- <sup>62</sup>S. S. Bystrov, V. V. Matveev, Y. S. Chernyshev, V. Balevičius, and V. I. Chizhik, "Molecular mobility in a set of imidazolium-based ionic liquids [bmim]<sup>+</sup>A<sup>-</sup> by the NMR-relaxation method," *J. Phys. Chem. B* **123**(10), 2362–2372 (2019).
- <sup>63</sup>Y. Shimizu, Y. Wachi, K. Fujii, M. Imanari, and K. Nishikawa, "NMR study on ion dynamics and phase behavior of a piperidinium-based room-temperature ionic liquid: 1-butyl-1-methylpiperidinium bis(fluorosulfonyl)amide," *J. Phys. Chem. B* **120**(25), 5710–5719 (2016).
- <sup>64</sup>J. H. Antony, D. Mertens, A. Dölle, P. Wasserscheid, and W. R. Carper, "Molecular reorientational dynamics of the neat ionic liquid 1-butyl-3-methylimidazolium hexafluorophosphate by measurement of <sup>13</sup>C nuclear magnetic relaxation data," *ChemPhysChem* **4**(6), 588–594 (2003).
- <sup>65</sup>P. M. Bayley, A. S. Best, D. R. MacFarlane, and M. Forsyth, "The effect of coordinating and non-coordinating additives on the transport properties in ionic liquid electrolytes for lithium batteries," *Phys. Chem. Chem. Phys.* **13**(10), 4632–4640 (2011).
- <sup>66</sup>K. Hayamizu, S. Tsuzuki, S. Seki, K. Fujii, M. Suenaga, and Y. Umebayashi, "Studies on the translational and rotational motions of ionic liquids composed of N-methyl-N-propyl-pyrrolidinium (P<sub>13</sub>) cation and bis(trifluoromethanesulfonyl)amide and bis(fluorosulfonyl)amide anions and their binary systems including lithium salts," *J. Chem. Phys.* **133**(19), 194505 (2010).
- <sup>67</sup>M. E. Di Pietro, F. Castiglione, and A. Mele, "Anions as dynamic probes for ionic liquid mixtures," *J. Phys. Chem. B* **124**(14), 2879–2891 (2020).